A Comprehensive Mechanistic Model for Upward Two-Phase Flow in Wellbores

A.M. Ansari, Pakistan Petroleum Ltd.; **N.D. Sylvester,** U. of Akron; and **C. Sarica, O. Shoham,** and **J.P. Brill,** U. of Tulsa

Summary. A comprehensive model is formulated to predict the flow behavior for upward two-phase flow. This model is composed of a model for flow-pattern prediction and a set of independent mechanistic models for predicting such flow characteristics as holdup and pressure drop in bubble, slug, and annular flow. The comprehensive model is evaluated by using a well data bank made up of 1,712 well cases covering a wide variety of field data. Model performance is also compared with six commonly used empirical correlations and the Hasan-Kabir mechanistic model. Overall model performance is in good agreement with the data. In comparison with other methods, the comprehensive model performed the best.

Introduction

Two-phase flow is commonly encountered in the petroleum, chemical, and nuclear industries. This frequent occurrence presents the challenge of understanding, analyzing, and designing two-phase systems.

Because of the complex nature of two-phase flow, the problem was first approached through empirical methods. The trend has shifted recently to the modeling approach. The fundamental postulate of the modeling approach is the existence of flow patterns or flow configurations. Various theories have been developed to predict flow patterns. Separate models were developed for each flow pattern to predict flow characteristics like holdup and pressure drop. By considering basic fluid mechanics, the resulting models can be applied with more confidence to flow conditions other than those used for their development.

Only Ozon et al.[1] and Hasan and Kabir[2] published studies on comprehensive mechanistic modeling of two-phase flow in vertical pipes. More work is needed to develop models that describe the physical phenomena more rigorously.

The purpose of this study is to formulate a detailed comprehensive mechanistic model for upward two-phase flow. The comprehensive model first predicts the existing flow pattern and then calculates the flow variables by taking into account the actual mechanisms of the predicted flow pattern. The model is evaluated against a wide range of experimental and field data available in the updated Tulsa U. Fluid Flow Projects (TUFFP) well data bank. The performance of the model is also compared with six empirical correlations and one mechanistic model used in the field.

Flow-Pattern Prediction

Taitel et al.[3] presented the basic work on mechanistic modeling of flow-pattern transitions for upward two-phase flow. They identified four distinct flow patterns (bubble, slug, churn, and annular flow) and formulated and evaluated the transition boundaries among them (**Fig. 1**). Barnea et al.[4] later modified the transitions to extend the applicability of the model to inclined flows. Barnea[5] then combined flow-pattern prediction models applicable to different inclination angle ranges into one unified model. Based on these different works, flow pattern can be predicted by defining transition boundaries among bubble, slug, and annular flows.

Bubble/Slug Transition. Taitel et al.[3] gave the minimum diameter at which bubble flow occurs as

$$d_{min} = 19.01 \left[\frac{(\rho_L - \rho_G)\sigma_L}{\rho_L^2 g} \right]^{1/2}. \qquad (1)$$

For pipes larger than this, the basic transition mechanism for bubble to slug flow is coalescence of small gas bubbles into large Taylor bubbles. This was found experimentally to occur at a void fraction

of about 0.25. Using this value of void fraction, we can express the transition in terms of superficial and slip velocities:

$$v_{Sg} = 0.25 v_s + 0.333 v_{SL}, \qquad (2)$$

where v_s is the slip or bubble-rise velocity given by[6]

$$v_s = 1.53 \left[\frac{g\sigma_L(\rho_L - \rho_G)}{\rho_L^2} \right]^{1/4}. \qquad (3)$$

This is shown as Transition A in **Fig. 2.**

Dispersed Bubble Transition. At high liquid rates, turbulent forces break large gas bubbles down into small ones, even at void fractions exceeding 0.25. This yields the transition to dispersed bubble flow[5]:

$$2 \left[\frac{0.4\sigma_L}{(\rho_L - \rho_G)g} \right]^{1/2} \left(\frac{\rho_L}{\sigma_L} \right)^{3/5} \left[\frac{f}{2d} \right]^{2/5} (v_{SL} + v_{Sg})^{1.2}$$

$$= 0.725 + 4.15 \left(\frac{v_{Sg}}{v_{Sg} + v_{SL}} \right)^{0.5}. \qquad (4)$$

This is shown as Transition B in Fig. 2.

At high gas velocities, this transition is governed by the maximum packing of bubbles to give coalescence. Scott and Kouba[7] concluded that this occurs at a void fraction of 0.76, giving the transition for no-slip dispersed bubble flow as

$$v_{Sg} = 3.17 v_{SL}. \qquad (5)$$

This is shown as Transition C in Fig. 2.

Transition to Annular Flow. The transition criterion for annular flow is based on the gas-phase velocity required to prevent the entrained liquid droplets from falling back into the gas stream. This gives the transition as

$$v_{Sg} = 3.1 \left[\frac{g\sigma_L(\rho_L - \rho_G)}{\rho_G^2} \right]^{1/4}, \qquad (6)$$

shown as Transition D in Fig. 2.

Barnea[5] modified the same transition by considering the effects of film thickness on the transition. One effect is that a thick liquid film bridged the gas core at high liquid rates. The other effect is instability of the liquid film, which causes downward flow of the film at low liquid rates. The bridging mechanism is governed by the minimum liquid holdup required to form a liquid slug:

$$H_{LF} > 0.12, \qquad (7)$$

where H_{LF} is the fraction of pipe cross section occupied by the liquid film, assuming no entrainment in the core. The mechanism of film instability can be expressed in terms of the modified Lockhart and Martinelli parameters, X_M and Y_M,
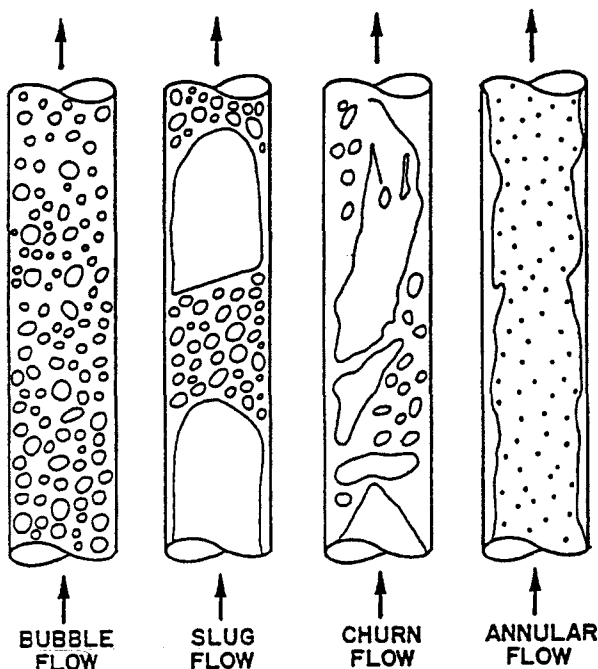
143

Fig. 1—Flow patterns in upward two-phase flow.

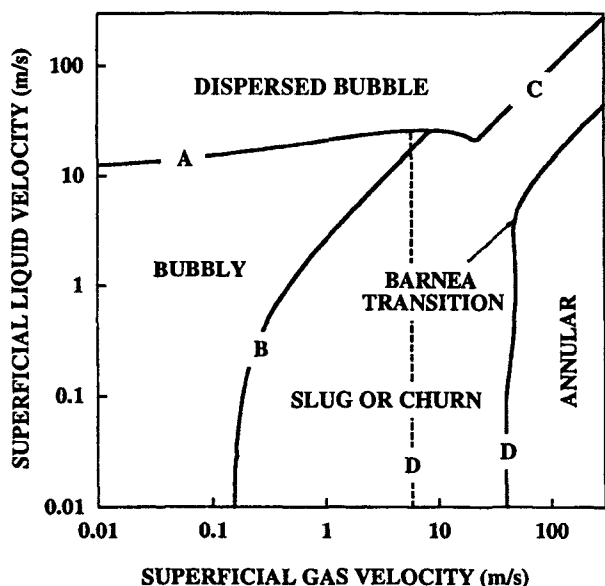**Fig. 2—Typical flow-pattern map for wellbores.**

$$Y_M = \frac{2-1.5H_{LF}}{H_{LF}^3(1-1.5H_{LF})}X_M^2, \qquad (8)$$

where $X_M = \sqrt{B\dfrac{\left(\dfrac{dp}{dL}\right)_{SL}}{\left(\dfrac{dp}{dL}\right)_{SC}}}$, ... (9)

$$Y_M = \frac{g \sin \theta(\rho_L-\rho_C)}{\left(\dfrac{dp}{dL}\right)_{SC}}, \qquad (10)$$

and $B=(1-F_E)^2(f_F/f_{SL})$. From geometric considerations, H_{LF} can be expressed in terms of minimum dimensionless film thickness, $\underline{\delta}_{min}$, as

$$H_{LF} = 4\underline{\delta}_{min}(1-\underline{\delta}_{min}) . \qquad (11)$$

To account for the effect of the liquid entrainment in the gas core, Eq. 7 is modified here as

$$\left(H_{LF} + \lambda_{LC}\frac{A_C}{A_P}\right) > 0.12. \qquad (12)$$

Annular flow exists if v_{Sg} is greater than that at the transition given by Eq. 6 and if the two Barnea criteria are satisfied. To satisfy the Barnea criteria, Eq. 8 must first be solved implicitly for δ_{min}. H_{LF} is then calculated from Eq. 11; if Eq. 12 is not satisfied, annular flow exists. Eq. 8 can usually be solved for δ_{min} by using a second-order Newton-Raphson approach. Thus, Eq. 8 can be expressed as

$$F(\underline{\delta}_{min}) = Y_M - \frac{2-1.5H_{LF}}{H_{LF}^3(1-1.5H_{LF})}X_M^2 \qquad (13)$$

and

$$F'(\underline{\delta}_{min}) = \frac{1.5H_{LF}'X_M^2}{H_{LF}^3(1-1.5H_{LF})}$$

$$+ \frac{(2-1.5H_{LF})X_M^2H_{LF}'(3-5.5H_{LF})}{H_{LF}^3(1-1.5H_{LF})^2}. \qquad (14)$$

The minimum dimensionless film thickness is then determined iteratively from

$$\underline{\delta}_{min_{j+1}} = \underline{\delta}_{min_j} - \frac{F(\underline{\delta}_{min_j})}{F'(\underline{\delta}_{min_j})}. \qquad (15)$$

A good initial guess is $\underline{\delta}_{min} = 0.25$.

Flow-Behavior Prediction

After the flow patterns are predicted, the next step is to develop physical models for the flow behavior in each flow pattern. This step resulted in separate models for bubble, slug, and annular flow. Churn flow has not yet been modeled because of its complexity and is treated as part of slug flow. The models developed for other flow patterns are discussed below.

Bubble Flow Model. The bubble flow model is based on Caetano's[8] work for flow in an annulus. The bubble flow and dispersed bubble flow regimes are considered separately in developing the model for the bubble flow pattern.

Because of the uniform distribution of gas bubbles in the liquid and no slippage between the two phases, dispersed bubble flow can be approximated as a pseudosingle phase. With this simplification, the two-phase parameters can be expressed as

$$\rho_{TP} = \rho_L\lambda_L + \rho_g(1-\lambda_L), \qquad (16)$$

$$\mu_{TP} = \mu_L\lambda_L + \mu_g(1-\lambda_L), \qquad (17)$$

and $v_{TP} = v_M v_{SL} + v_{Sg}$, ... (18)

where $\lambda_L = v_{SL}/v_m$. .... (19)

For bubble flow, the slippage is considered by taking into account the bubble-rise velocity relative to the mixture velocity. By assuming a turbulent velocity profile for the mixture with the rising bubble concentrated more at the center than along the pipe wall, we can express the slippage velocity as

$$v_S = v_g - 1.2v_m . \qquad (20)$$

Harmathy[6] gave an expression for bubble-rise velocity (Eq. 3). To account for the effect of bubble swarm, Zuber and Hench[9] modified this expression:

$$v_S = 1.53\left[\frac{g\sigma_L(\rho_L-\rho_g)}{\rho_L^2}\right]^{1/4}H_L^{n'}, \qquad (21)$$
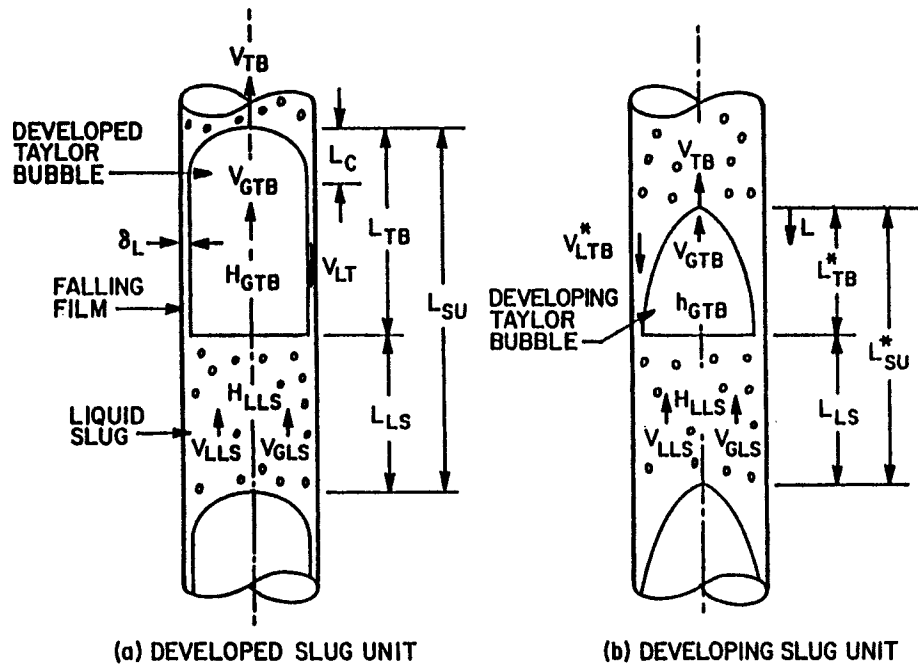
Fig. 3—Schematic of slug flow.

where the value of n' varies from one study to another. In the present study, $n'=0.5$ was used to give the best results. Thus, Eq. 20 yields

$$1.53\left[\frac{g\sigma_L(\rho_L-\rho_g)}{\rho_L^2}\right]^{\frac{1}{4}} H_L^{0.5} = \frac{v_{Sg}}{1-H_L}-1.2v_M. \quad\quad\quad (22)$$

This gives an implicit equation for the actual holdup for bubble flow. The two-phase flow parameters can now be calculated from

$$\rho_{TP} = \rho_L H_L + \rho_g(1-H_L) \quad\quad\quad\quad\quad (23)$$

and $\mu_{TP} = \mu_L H_L + \mu_g(1-H_L)$. $\quad\quad\quad\quad (24)$

The two-phase pressure gradient is made up of three components. Thus,

$$\left(\frac{dp}{dL}\right) = \left(\frac{dp}{dL}\right)_e + \left(\frac{dp}{dL}\right)_f + \left(\frac{dp}{dL}\right)_a. \quad\quad\quad (25)$$

The elevation pressure gradient is given by

$$\left(\frac{dp}{dL}\right)_e = \rho_{TP}g\sin\theta. \quad\quad\quad\quad\quad (26)$$

The friction component is given by

$$\left(\frac{dp}{dL}\right)_f = \frac{f_{TP}\rho_{TP}v_{TP}^2}{2d}, \quad\quad\quad\quad\quad (27)$$

where f_{TP} is obtained from a Moody diagram for a Reynolds number defined by

$$N_{Re_{TP}} \frac{\rho_{TP}v_{TP}d}{\mu_{TP}}. \quad\quad\quad\quad\quad\quad (28)$$

Because bubble flow is dominated by a relatively incompressible liquid phase, there is no significant change in the density of the flowing fluids. This keeps the fluid velocity nearly constant, resulting in essentially no pressure drop owing to acceleration. Therefore, the acceleration pressure drop is safely neglected, compared with the other pressure drop components.

Slug Flow Model. Fernandes et al.[10] developed the first thorough physical model for slug flow. Sylvester[11] presented a simplified ver-

sion of this model. The basic simplification was the use of a correlation for slug void fraction. These models used an important assumption of fully developed slug flow. McQuillan and Whalley[12] introduced the concept of developing flow during their study of flow-pattern transitions. Because of the basic difference in flow geometry, the model treats fully developed and developing flow separately.

For a fully developed slug unit (**Fig. 3a**), the overall gas and liquid mass balances give

$$v_{Sg} = \beta v_{gTB}(1-H_{LTB}) + (1-\beta)v_{gLS}(1-H_{LLS}) \quad\quad (29)$$

and $v_{SL} = (1-\beta)v_{LLS}H_{LLS} - \beta V_{LTB}H_{LTB}, \quad\quad\quad (30)$

respectively, where

$$\beta = L_{TB}/L_{SU}. \quad\quad\quad\quad\quad\quad\quad (31)$$

Mass balances for liquid and gas from liquid slug to Taylor bubble give

$$(v_{TB}cc-v_{LLS})H_{LLS} = [v_{TB}-(-V_{LTB})]H_{LTB} \quad\quad (32)$$

and $(v_{TB}-v_{gLS})(1-H_{LLS}) = (v_{TB}-v_{gTB})(1-H_{LTB}). \quad\quad (33)$

The Taylor bubble-rise velocity is equal to the centerline velocity plus the Taylor bubble-rise velocity in a stagnant liquid column; i.e.,

$$v_{TB} = 1.2v_m + 0.35\left[\frac{gd(\rho_L-\rho_g)}{\rho_L}\right]^{\frac{1}{2}}. \quad\quad\quad (34)$$

Similarly, the velocity of the gas bubbles in the liquid slug is

$$v_{gLS} = 1.2v_m + 1.53\left[\frac{g\sigma_L(\rho_L-\rho_g)}{\rho_L^2}\right]^{\frac{1}{4}} H_{LLS}^{0.5}, \quad\quad (35)$$

where the second term on the right side represents the bubble-rise velocity defined in Eq. 21.

The velocity of the falling film can be correlated with the film thickness with the Brotz[13] expression,

$$v_{LTB} = \sqrt{196.7g\delta_L}, \quad\quad\quad\quad\quad\quad (36)$$

where δ_L, the constant film thickness for developed flow, can be expressed in terms of Taylor bubble void fraction to give

$$v_{LTB} = 9.916\left[gd\left(1-\sqrt{H_{gTB}}\right)\right]^{\frac{1}{2}}. \quad\quad\quad (37)$$

The liquid slug void fraction can be obtained by Sylvester's[11] correlation and from Fernandes et al.'s[10] and Schmidt's[14] data,

$$H_{gLS} = \frac{v_{Sg}}{0.425 + 2.65v_m}. \quad \dots\dots\dots\dots\dots\dots\dots\dots\dots (38)$$

Eqs. 29 or 30, 31 through 35, 37, and 38 can be solved iteratively to obtain the following eight unknowns that define the slug flow model: β, H_{LTB}, H_{gLS}, v_{gTB}, v_{LTB}, v_{gLS}, v_{LLS}, and v_{TB}. Vo and Shoham[15] showed that these eight equations can be combined algebraically to give

$$\left(9.916\sqrt{gd}\right)\left(1-\sqrt{1-H_{LTB}}\right)^{0.5}H_{LTB}-v_{TB}(1-H_{LTB}) + \tilde{A} = 0,$$

$$\dots\dots\dots\dots\dots\dots\dots\dots\dots (39)$$

where $\tilde{A} = H_{gLS}v_{TB} + (1-H_{gLS})$

$$\times \left[v_m - H_{gLS}\left\{ 1.53\left[\frac{\sigma_L g(\rho_L-\rho_g)}{\rho_L^2}\right]^{0.25}(1-H_{gLS})^{0.5}\right\}\right].$$

$$\dots\dots\dots\dots\dots\dots\dots\dots\dots (40)$$

With v_{TB} and H_{gLS} given by Eqs. 34 and 38, respectively, $\tilde{A}$ can be readily determined from Eq. 40. Eq. 39 is then used to find H_{LTB} with an iterative solution method. Defining the left side of Eq. 39 as $F(H_{LTB})$, then

$$F(H_{LTB}) = \left(9.916\sqrt{gd}\right)\left(1-\sqrt{1-H_{LTB}}\right)^{0.5}H_{LTB}-v_{TB}(1-H_{LTB}) + \tilde{A}.$$

$$\dots\dots\dots\dots\dots\dots\dots\dots\dots (41)$$

Taking the derivative of Eq. 41 with respect to H_{LTB} yields

$$F'(H_{LTB}) = v_{TB} + \left(9.916\sqrt{gd}\right)$$

$$\times \left[\left(1-\sqrt{1-H_{LTB}}\right)^{0.5} + \frac{H_{LTB}}{4\sqrt{(1-H_{LTB})\left(1-\sqrt{1-H_{LTB}}\right)}}\right].$$

$$\dots\dots\dots\dots\dots\dots\dots\dots\dots (42)$$

H_{LTB}, the root of Eq. 39, is then determined iteratively from

$$H_{LTB_{j+1}} = H_{LTB_j} - \frac{F(H_{LTB_j})}{F'(H_{LTB_j})}. \quad \dots\dots\dots\dots\dots\dots\dots\dots (43)$$

The step-by-step procedure for determining all slug flow variables is as follows.
1. Calculate v_{TB} and H_{gLS} from Eqs. 34 and 38.
2. Using Eqs. 40 through 43, determine H_{LTB}. A good initial guess is $H_{LTB}=0.15$.
3. Solve Eq. 37 for v_{LTB}. Note that $H_{gTB}=1-H_{LTB}$.
4. Solve Eq. 32 for v_{LLS}. Note that $H_{LLS}=1-H_{gLS}$.
5. Solve Eq. 35 for v_{gLS}.
6. Solve Eq. 33 for v_{gTB}.
7. Solve Eq. 29 or 30 for β.
8. Assuming that $L_{LS}=30d$, calculate L_{SU} and L_{TB} from the definition of β.

To model developing slug flow, as in **Fig. 3b**, we must determine the existence of such flow. This requires calculating and comparing the cap length with the total length of a developed Taylor bubble. The expression for the cap length is[12]

$$L_c = \frac{1}{2g}\left[v_{TB} + \frac{v_{NgTB}}{H_{NLTB}}(1-H_{NLTB}) - \frac{v_m}{H_{NLTB}}\right]^2, \quad \dots\dots\dots (44)$$

where v_{NgTB} and H_{NLTB} are calculated at the terminal film thickness (called Nusselt film thickness) given by

$$\delta_N = \left[\frac{3}{4}d\frac{v_{NLTB}\mu_L(1-H_{NLTB})}{g(\rho_L-\rho_g)}\right]^{1/3}. \quad \dots\dots\dots\dots\dots (45)$$

The geometry of the film flow gives H_{NLTB} in terms of δ_N as

$$H_{NLTB} = 1-\left(1-\frac{2\delta_N}{d}\right)^2. \quad \dots\dots\dots\dots\dots\dots\dots (46)$$

To determine v_{NgTB}, the net flow rate of δ_N can be used to obtain

$$v_{NgTB} = v_{TB}-(v_{TB}-v_{gLS})\frac{(1-H_{LLS})}{(1-H_{NLTB})}. \quad \dots\dots\dots\dots (47)$$

The length of the liquid slug can be calculated empirically from

$$L_{LS} = C'd, \quad \dots\dots\dots\dots\dots\dots\dots\dots\dots\dots\dots\dots\dots (48)$$

where C' was found[16] to vary from 16 to 45. We use $C'=30$ in this study. This gives the Taylor bubble length as

$$L_{TB} = [L_{LS}/(1-\beta)]\beta. \quad \dots\dots\dots\dots\dots\dots\dots\dots\dots (49)$$

From the comparison of L_c and L_{TB}, if $L_c \geq L_{TB}$, the flow is developing slug flow. This requires new values for L_{TB}^*, H_{LTB}^*, and v_{LTB}^* calculated earlier for developed flow.

For L_{TB}^*, Taylor bubble volume can be used:

$$V_{gTB}^* = \int_0^{L_{TB}^*} A_{TB}^*(L)dL, \quad \dots\dots\dots\dots\dots\dots\dots\dots (50)$$

where A_{TB}^* can be expressed in terms of local holdup $h_{LTB}(L)$, which in turn can be expressed in terms of velocities by using Eq. 32. This gives

$$A_{TB}^*(L) = \left[1-\frac{(v_{TB}-v_{LLS})H_{LLS}}{\sqrt{2gL}}\right]A_p. \quad \dots\dots\dots\dots (51)$$

The volume can be expressed in terms of flow geometry as

$$V_{gTB}^* = v_{Sg}A_p\left(\frac{L_{TB}^* + L_{LS}}{v_{TB}}\right) - v_{gLS}A_p(1-H_{LLS})\frac{L_{LS}}{v_{TB}}. \quad \dots\dots (52)$$

Substitution of Eqs. 51 and 52 into Eq. 50 gives

$$v_{Sg}\left(\frac{L_{TB}^* + L_{LS}}{v_{TB}}\right) - v_{gLS}(1-H_{LLS})\frac{L_{LS}}{v_{TB}}$$

$$= \int_0^{L_{TB}^*}\left[1-\frac{(v_{TB}-v_{LLS})H_{LLS}}{\sqrt{2gL}}\right]dL. \quad \dots\dots\dots\dots\dots (53)$$

Eq. 53 can be integrated and then simplified to give

$$L_{TB}^{*2} + \left(\frac{-2ab-4c^2}{a^2}\right)L_{TB}^* + \frac{b^2}{a^2} = 0, \quad \dots\dots\dots\dots\dots (54)$$

where $a=1-v_{Sg}/v_{TB}$, $\dots\dots\dots\dots\dots\dots\dots\dots\dots (55)$

$$b = \frac{v_{Sg}-v_{gLS}(2-H_{LLS})}{v_{TB}}L_{LS}, \quad \dots\dots\dots\dots\dots\dots\dots (56)$$

and $c = \frac{v_{TB}-v_{LLS}}{\sqrt{2g}}H_{LLS}. \quad \dots\dots\dots\dots\dots\dots\dots\dots (57)$

After calculating L_{TB}^*, the other local parameters can be calculated from

$$v_{LTB}^*(L) = \sqrt{2gL}-v_{TB} \quad \dots\dots\dots\dots\dots\dots\dots\dots\dots (58)$$

and $h_{LTB}^*(L) = \frac{(v_{TB}-v_{LLS})H_{LLS}}{\sqrt{2gL}}. \quad \dots\dots\dots\dots\dots\dots (59)$

In calculating pressure gradients, we consider the effect of varying film thickness and neglect the effect of friction along the Taylor bubble.

For developed flow, the elevation component occurring across a slug unit is given by

$$\left(\frac{dp}{dL}\right)_e = [(1-\beta)\rho_{LS} + \beta\rho_g]g\sin\theta, \dots\dots\dots\dots\dots (60)$$

where $\rho_{LS} = \rho_L H_{LLS} + \rho_g(1-H_{LLS})$. $\dots\dots\dots\dots (61)$

The elevation component for developing slug flow is given by

$$\left(\frac{dp}{dL}\right)_e = [(1-\beta^*)\rho_{LS} + \beta^*\rho_{TBA}]g\sin\theta, \dots\dots\dots\dots (62)$$

where ρ_{TBA} is based on average void fraction in the Taylor bubble section with varying film thickness. It is given by

$$\rho_{TBA} = \rho_L H_{LTBA} + \rho_g(1-H_{LTBA}), \dots\dots\dots\dots (63)$$

where H_{LTBA} is obtained by integrating Eq. 59 and dividing by L_{TB}^*, giving

$$H_{LTBA} = \frac{2(v_{TB}-v_{LLS})H_{LLS}}{\sqrt{2gL_{TB}^*}} . \dots\dots\dots\dots\dots (64)$$

The friction component is the same for both the developed and developing slug flows because it occurs only across the liquid slug. This is given as

$$\left(\frac{dp}{dL}\right)_f = \frac{f_{LS}\rho_{LS}v_m^2}{2d}(1-\beta), \dots\dots\dots\dots\dots (65)$$

where β should be replaced by β^* for developing flow. f_{LS} can be calculated by using

$$N_{Re_{LS}} = \rho_{LS}v_m d/\mu_{LS}. \dots\dots\dots\dots\dots (66)$$

For the pressure gradient due to acceleration, the velocity in the film must be considered. The liquid in the slug experiences deceleration as its upward velocity of v_{LLS} changes to a downward velocity of v_{LTB}. The same liquid also experiences acceleration when it exits from the film with a velocity v_{LTB} into an upward moving liquid slug of velocity v_{LLS}. If the two changes in the liquid velocity occur within the same slug unit, then no net pressure drop due to acceleration exists over that slug unit. This happens when the slug flow is stable. The correlation used for slug length is based on its stable length, so the possibility of a net pressure drop due to acceleration does not exist. Therefore, no acceleration component of pressure gradient is considered over a slug unit.

Annular Flow Model. A discussion on the hydrodynamics of annular flow was presented by Wallis.[17] Along with this, Wallis also presented the classic correlations for entrainment and interfacial friction as a function of film thickness. Later, Hewitt and Hall-Taylor[18] gave a detailed analysis of the mechanisms involved in an annular flow. All the models that followed later are based on this approach.

A fully developed annular flow is shown in **Fig 4.** The conservation of momentum applied separately to the core and the film yields

$$A_c\left(\frac{dp}{dL}\right)_c -\tau_i S_i -\rho_c A_c g\sin\theta = 0 \dots\dots\dots\dots (67)$$

and $A_F\left(\frac{dp}{dL}\right)_F + \tau_i S_i -\tau_F S_F -\rho_L A_F g\sin\theta = 0. \dots\dots (68)$

The core density, ρ_c, is a no-slip density because the core is considered a homogeneous mixture of gas and entrained liquid droplets flowing at the same velocity. Thus,

$$\rho_c = \rho_L \lambda_{LC} + \rho_g(1-\lambda_{LC}), \dots\dots\dots\dots (69)$$

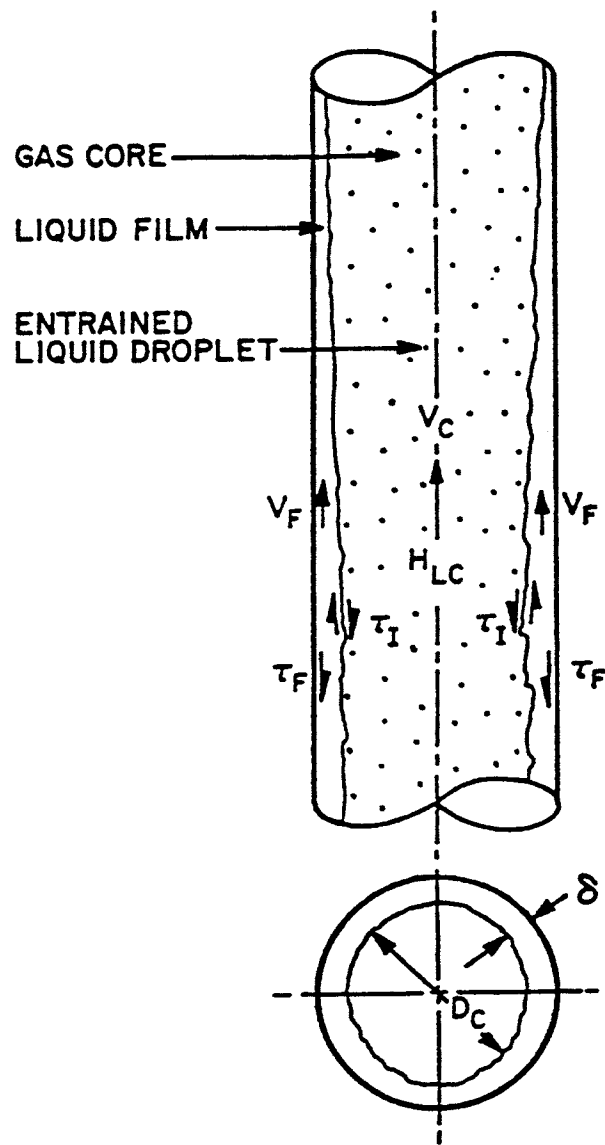where $\lambda_{LC} = \dfrac{F_E v_{SL}}{v_{Sg} + F_E v_{SL}}. \dots\dots\dots\dots\dots (70)$

Fig. 4—Schematic of annular flow.

F_E is the fraction of the total liquid entrained in the core, given by Wallis as

$$F_E = 1-\exp[-0.125(v_{crit}-1.5)], \dots\dots\dots\dots (71)$$

where $v_{crit} = 10,000\dfrac{v_{Sg}\mu_g}{\sigma_L}\left(\dfrac{\rho_g}{\rho_L}\right)^{\frac{1}{2}}. \dots\dots\dots\dots (72)$

The shear stress in the film can be expressed as

$$\tau_F = f_F\rho_L\frac{v_F^2}{8}, \dots\dots\dots\dots\dots (73)$$

where f_F is obtained from a Moody diagram for a Reynolds number defined by

$$N_{Re_F} = \frac{\rho_L v_F d_{HF}}{\mu_L}, \dots\dots\dots\dots\dots (74)$$

where $v_F = \dfrac{q_L(1-F_E)}{A_F} = \dfrac{v_{SL}(1-F_E)}{4\delta(1-\delta)} \dots\dots\dots\dots (75)$

and $d_{HF} = 4\delta(1-\delta)d. \dots\dots\dots\dots\dots (76)$

This gives

$$\tau_F = \frac{f_F}{8}(1-F_E)^2\rho_L\left[\frac{v_{SL}}{4\delta(1-\delta)}\right]^2. \dots\dots\dots\dots (77)$$

Eq. 77 reduces to

$$\tau_F = \frac{d}{4} \frac{(1-F_E)^2}{[4\underline{\delta}(1-\underline{\delta})]^2 f_{SL}} \frac{f_F}{\left(\frac{dp}{dL}\right)_{SL}}, \dots \dots \dots \dots (78)$$

where the superficial liquid friction pressure gradient is given by

$$\left(\frac{dp}{dL}\right)_{SL} = \frac{f_{SL}\rho_L v_{SL}^2}{2d}. \dots \dots \dots \dots \dots \dots (79)$$

f_{SL} is the friction factor for superficial liquid velocity and can be obtained from a Moody diagram for a Reynolds number defined by

$$N_{Re_{SL}} = \rho_L v_{SL} d / \mu_L. \dots \dots \dots \dots \dots \dots (80)$$

For the shear stress at the interface,

$$\tau_i = f_i \, \rho_c v_c^2 / 8, \dots \dots \dots \dots \dots \dots (81)$$

where $v_c = v_{SC}/(1-2\underline{\delta})^2 \dots \dots \dots \dots \dots \dots (82)$

and $f_i = f_{SC} Z, \dots \dots \dots \dots \dots \dots (83)$

where Z is a correlating factor for interfacial friction and the film thickness. Based on the performance of the model, the Wallis expression for Z works well for thin films or high entrainments, whereas the Whalley and Hewitt[19] expression is good for thick films or low entrainments. Thus,

$$Z = 1 + 300\underline{\delta} \quad \text{for } F_E > 0.9 \dots \dots \dots \dots (84)$$

and $Z = 1 + 24\left(\frac{\rho_g}{\rho_g}\right)^{1/3} \underline{\delta} \quad \text{for } F_E < 0.9. \dots \dots \dots (85)$

Combining Eqs. 81 through 83 yields

$$\tau_i = \frac{d}{4} \frac{Z}{(1-2\underline{\delta})^4} \left(\frac{dp}{dL}\right)_{SC}. \dots \dots \dots \dots (86)$$

The superficial friction pressure gradient in the core is given by

$$\left(\frac{dp}{dL}\right)_{SC} = \frac{f_{SC}\rho_c v_{SC}^2}{2d}, \dots \dots \dots \dots \dots \dots (87)$$

where f_{SC} is obtained from a Moody diagram for a Reynolds number defined by

$$N_{Re_{SC}} = \rho_c v_{sc} d / \mu_{sc}, \dots \dots \dots \dots \dots \dots (88)$$

$$v_{SC} = F_E v_{SL} + v_{Sg}, \dots \dots \dots \dots \dots \dots (89)$$

and $\mu_C = \mu_L \lambda_{LC} + \mu_g(1-\lambda_{LC}). \dots \dots \dots \dots (90)$

The pressure gradient for annular flow can be calculated by substituting the above equations into Eqs. 67 and 68. Thus,

$$\left(\frac{dp}{dL}\right)_C = \frac{Z}{(1-2\underline{\delta})^5} \left(\frac{dp}{dL}\right)_{SC} + \rho_C g \sin \theta \dots \dots \dots (91)$$

and $\left(\frac{dp}{dL}\right)_F = \frac{(1-F_E)^2}{64\underline{\delta}^3(1-\underline{\delta})^3} \left(\frac{f_F}{f_{SL}}\right)\left(\frac{dp}{dL}\right)_{SL}$

$$-\frac{Z}{4\underline{\delta}(1-\underline{\delta})(1-2\underline{\delta})^3} \left(\frac{dp}{dL}\right)_{SC} + \rho_L g \sin \theta. \dots \dots \dots (92)$$

The basic unknown in the above equations is the dimensionless film thickness, $\underline{\delta}$. An implicit equation for $\underline{\delta}$ can be obtained by equating Eqs. 91 and 92. This gives

$$\frac{Z}{4\underline{\delta}(1-\underline{\delta})(1-2\underline{\delta})^5} \left(\frac{dp}{dL}\right)_{SC} -(\rho_L - \rho_C)g \sin \theta$$

$$-\frac{(1-FE)^2}{64\underline{\delta}^3(1-\underline{\delta})^3 f_{SL}} \frac{f_F}{\left(\frac{dp}{dL}\right)_{SL}} = 0. \dots \dots \dots \dots (93)$$

To simplify this equation, the dimensionless approach developed by Alves et al.[20] is used. This approach defines the following dimensionless groups in addition to previously defined modified Lockhart Martinelli parameters, X_M and Y_M.

$$\phi_C^2 = \frac{(dp/dL)_C - g\rho_C \sin \theta}{(dp/dL)_{SC}}. \dots \dots \dots \dots (94)$$

and $\phi_F^2 = \frac{(dp/dL)_F - g\rho_L \sin \theta}{(dp/dL)_{SL}}. \dots \dots \dots \dots (95)$

By using the modified Lockhart Martinelli parameters, Eq. 93 reduces to

$$Y_M - \frac{Z}{4\underline{\delta}(1-\underline{\delta})[1-4\underline{\delta}(1-\underline{\delta})]^{2.5}} + \frac{X_M^2}{[4\underline{\delta}(1-\underline{\delta})]^3} = 0. \dots \dots (96)$$

The above equations can be solved iteratively to obtain $\underline{\delta}$. If Eq. 96 is $F(\underline{\delta})$, then taking the derivative of Eq. 96 with respect to $\underline{\delta}$ yields

$$F'(\underline{\delta}) = \frac{Z[4(1-2\underline{\delta})]}{[4\underline{\delta}(1-\underline{\delta})]^2[1-4\underline{\delta}(1-\underline{\delta})]^{2.5}}$$

$$-\frac{Z'}{4\underline{\delta}(1-\underline{\delta})[1-4\underline{\delta}(1-\underline{\delta})]^{2.5}}$$

$$-\frac{2.5Z[4(1-2\underline{\delta})]}{4\underline{\delta}(1-\underline{\delta})[1-4\underline{\delta}(1-\underline{\delta})]^{3.5}} - \frac{3X_M^2[4(1-2\underline{\delta})]}{[4\underline{\delta}(1-\underline{\delta})]^4}. \dots \dots (97)$$

The Newton-Raphson method can be incorporated to determine $\underline{\delta}$, the root of Eq. 96. Thus,

$$\underline{\delta}_{j+1} = \underline{\delta}_j - \frac{F(\underline{\delta}_j)}{F'(\underline{\delta}_j)}. \dots \dots \dots \dots \dots \dots (98)$$

Once $\underline{\delta}$ is known, the dimensionless groups ϕ_F and ϕ_C can be obtained from the following form of Eqs. 91 and 92

$$\phi_C^2 = \frac{Z}{(1-2\underline{\delta})^5} \dots \dots \dots \dots \dots \dots (99)$$

and $\phi_F^2 = \frac{(1-FE)^2}{[1-(1-2\underline{\delta})^2]^2 f_{SL}} \frac{f_F}{} x$

$$\left\{ \frac{\frac{Z}{(1-2\underline{\delta})^5} - Y_M}{\frac{Z}{(1-2\underline{\delta})^5} - Y_M[1-(1-2\underline{\delta})^2]^2} \right\}. \dots \dots \dots \dots (100)$$

Alves[20] stated that Eq. 100 can be expressed as

$$\phi_F^2 = \frac{\phi_C^2 - Y_M}{X_M^2}. \dots \dots \dots \dots \dots \dots (101)$$

The total pressure gradient can then be obtained from either Eq. 94 or 95 because the pressure gradient in the film and core must be the same. Thus,

$$\left(\frac{dp}{dL}\right)_T = \left(\frac{dp}{dL}\right)_C = \phi_C^2 \left(\frac{dp}{dL}\right)_{SC} + g\rho_C \sin \theta \dots \dots \dots (102)$$

or $\left(\frac{dp}{dL}\right)_T = \left(\frac{dp}{dL}\right)_F = \phi_F^2 \left(\frac{dp}{dL}\right)_{SL} + g\rho_L \sin \theta. \dots \dots \dots (103)$

Note that the above total pressure gradient equations do not include accelerational pressure gradient. This is based on results found by Lopes and Dukler[21] indicating that, except for a limited range of high liquid flow rates, the accelerational component result-

TABLE 1—RANGE OF WELL DATA				
Source	Nominal Diameter (in.)	Oil Rate (STB/D)	Gas Rate (MSCF/D)	Oil Gravity (°API)
Old TUFFP* Data Bank	1 to 8	0 to 10,150	1.5 to 10,567	9.5 to 70.5
Govier and Fogarasi[22]	2 to 4	8 to 1,600	114 to 27,400	17 to 112
Asheim[23]	$2^7/_8$ to 6	720 to 27,000	740 to 55,700	35 to 86
Chierici et al.[24]	$2^7/_8$ to 5	0.3 to 69	6 to 27,914	8.3 to 46
Prudhoe Bay	5½ to 7	600 to 23,000	200 to 110,000	24 to 86

*Includes data from Poettmann and Carpenter,[25] Fancher and Brown,[26] Hagedorn,[27] Baxendell and Thomas,[28] Orkiszewski,[29] Espanol,[30] Messulam,[31] Camacho,[32] and field data from several oil companies.

ing from the exchange of liquid droplets between the core and the film is negligible.

Evaluation

The evaluation of the comprehensive model is carried out by comparing the pressure drop from the model with the measured data in the updated TUFFP well data bank that comprises 1,712 well cases with a wide range of data, as given in **Table 1**. The performance of the model is also compared with that of six correlations and another mechanistic model that are commonly used in the petroleum industry.

Criteria for Comparison with Data

The evaluation of the model using the data bank is based on the following statistical parameters.

Average percent error:

$$E_1 = \left(\frac{1}{n} \sum_{i=1}^{n} e_{ri}\right) \times 100, \quad \ldots\ldots\ldots\ldots\ldots\ldots\ldots \quad (104)$$

where $e_{ri} = \dfrac{\Delta p_{icalc} - \Delta p_{imeas}}{\Delta p_{imeas}}. \quad \ldots\ldots\ldots\ldots\ldots\ldots\ldots \quad (105)$

E_1 indicates the overall trend of the performance, relative to the measured pressure drop.

Absolute average percentage error:

$$E_2 = \left(\frac{1}{n} \sum_{i=1}^{n} |e_{ri}|\right) \times 100. \quad \ldots\ldots\ldots\ldots\ldots\ldots \quad (106)$$

E_2 indicates how large the errors are on the average.

Percent standard deviation:

$$E_3 = \sum_{i=1}^{n} \sqrt{\frac{(e_{ri} - E_1)^2}{n-1}}. \quad \ldots\ldots\ldots\ldots\ldots\ldots \quad (107)$$

E_3 indicates the degree of scattering of the errors about their average value.

Average error:

$$E_4 = \left(\frac{1}{n} \sum_{i=1}^{n} e_i\right), \quad \ldots\ldots\ldots\ldots\ldots\ldots\ldots \quad (108)$$

where $e_i = \Delta p_{icalc} - \Delta p_{imeas}. \quad \ldots\ldots\ldots\ldots\ldots\ldots \quad (109)$

E_4 indicates the overall trend independent of the measured pressure drop.

Absolute average error:

$$E_5 = \left(\frac{1}{n} \sum_{i=1}^{n} |e_i|\right). \quad \ldots\ldots\ldots\ldots\ldots\ldots \quad (110)$$

E_5 is also independent of the measured pressure drop and indicates the magnitude of the average error.

Standard deviation:

$$E_6 = \sum_{i=1}^{n} \sqrt{\frac{(e_i - E_4)^2}{n-1}}. \quad \ldots\ldots\ldots\ldots\ldots\ldots \quad (111)$$

E_6 indicates the scattering of the results, independent of the measured pressure drop.

Criteria for Comparison With Other Correlations and Models

The correlations and models used for the comparison are a modified Hagedorn and Brown,[27] Duns and Ros,[33] Orkiszewski[29] with Trig-gia correction,[34] Beggs and Brill[35] with Palmer correction,[36] Mukherjee and Brill,[37] Aziz et al.,[38] and Hasan and Kabir.[2,39] The comparison is accomplished by comparing the statistical parameters. The comparison involves the use of a relative performance factor defined by

$$F_{rp} = \frac{|E_1| - |E_{1_{min}}|}{|E_{1_{max}}| - |E_{1_{min}}|} + \frac{E_2 - E_{2_{min}}}{E_{2_{max}} - E_{2_{min}}}$$

TABLE 2—RELATIVE PERFORMANCE FACTORS											
	EDB	VW	DW	VNH	ANH	AB	AS	VS	SNH	VSNH	AAN
n	1712	1086	626	755	1381	29	1052	654	745	387	70
MODEL	0.700	1.121	1.378	0.081	0.000	0.143	1.295	1.461	0.112	0.142	0.000
HAGBR	0.585	0.600	0.919	0.876	0.774	2.029	0.386	0.485	0.457	0.939	0.546
AZIZ	1.312	1.108	2.085	0.803	1.062	0.262	1.798	1.764	1.314	1.486	0.214
DUNRS	1.719	1.678	1.678	1.711	1.792	1.128	2.056	2.028	1.852	2.296	1.213
HASKA	1.940	2.005	2.201	1.836	1.780	0.009	2.575	2.590	2.044	1.998	1.043
BEGBR	2.982	2.908	3.445	3.321	3.414	2.828	2.883	2.595	3.261	3.282	1.972
ORKIS	4.284	5.273	2.322	5.838	4.688	1.226	3.128	3.318	3.551	4.403	6.000
MUKBR	4.883	4.647	6.000	3.909	4.601	4.463	5.343	5.140	4.977	4.683	1.516

EBD=entire databank; VW=vertical well cases; DW=deviated well cases; VNH=vertical well cases without Hagedorn and Brown data; ANH=all well cases without Hagedorn and Brown data; AB=all well cases with 75% bubble flow; AS=all well cases with 100% slug flow; VS=vertical well cases with 100% slug flow; SNH=all well cases with 100% slug flow without Hagedorn and Brown data; AAN=all well cases with 100% annular flow; HAGBR=Hagedorn and Brown correlation; AZIZ=Aziz et al. correlation; DUNRS=Duns and Ros correlation; HASKA=Hasan and Kabir mechanistic model; BEGBR=Beggs and Brill correlation; ORKIS=Orkiszewski correlation; MUKBR=Mukherjee and Brill correlation.

$$+ \frac{E_3 - E_{3_{min}}}{E_{3_{max}} - E_{3_{min}}} + \frac{|E_4| - |E_{4_{min}}|}{|E_{4_{max}}| - |E_{4_{min}}|}$$

$$+ \frac{E_5 - E_{5_{min}}}{E_{5_{max}} - E_{5_{min}}} + \frac{E_6 - E_{6_{min}}}{E_{6_{max}} - E_{6_{min}}}. \quad \dots \dots \dots \dots \dots \dots \dots \dots \text{(112)}$$

The minimum and maximum possible values for F_{rp} are 0 and 6, indicating the best and worst performances, respectively.

The evaluation of the model in terms of F_{rp} is given in **Table 2**, with the best value for each column being boldfaced.

Overall Evaluation. The overall evaluation involves the entire comprehensive model so as to study the combined performance of all the independent flow pattern behavior models together. The evaluation is first performed by using the entire data bank, resulting in Col. 1 of Table 2. Model performance is also checked for vertical well cases only, resulting in Col. 2 of Table 2, and for deviated well cases only, resulting in Col. 3 of Table 2. To make the comparison unbiased with respect to the correlations, a second database was created that excluded 331 sets of data from the Hagedorn and Brown study. For this reduced data bank, the results for all vertical well cases are shown in Col. 4 of Table 2, and the results for combined vertical and deviated well cases are shown in Col. 5 of Table 2.

Evaluation of Individual Flow Pattern Models. The performance of individual flow pattern models is based on sets of data that are dominant in one particular flow pattern, as predicted by the transitions described earlier. For the bubble flow model, well cases with bubble flow existing for more than 75% of the well length are considered in order to have an adequate number of cases. These results are shown in Col. 6 of Table 2. Cols. 7 through 10 of Table 2 give results for well cases predicted to have slug flow exist for 100% of the well length. The cases used for Col. 7 and 8 were selected from the entire data bank, whereas the cases used for Cols. 9 and 10 and 11 were selected from the reduced data bank that eliminated the Hagedorn and Brown data, which is one-third of all the vertical well cases. Finally, Col. 11 of Table 2 gives results for those cases in the total data bank that were predicted to be in annular flow for 100% of the well length.

Complete performance results of each model or correlation against individual statistical parameters (E_1, E_6) are given in the supplement to this paper.[40]

Conclusions

From Cols. 1 through 11 of Table 2, the performance of the model and other empirical correlations indicates the following.

1. The overall performance of the comprehensive model is superior to all other methods considered. However, the overall performances of the Hagedorn and Brown, Aziz *et al.*, Duns and Ros, and Hasan and Kabir models are comparable to that of the model. For the last three, this can be attributed to the use of flow mechanisms in these methods. The excellent performance of the Hagedorn and Brown correlation can be explained only by the extensive data used in its development and modifications made to the correlation. In fact, when the data without Hagedorn and Brown well cases are considered, the model performed the best (Cols. 4 and 5).

2. Although the Hagedorn and Brown correlation performed better than the other correlations and models for deviated wells, none of the methods gave satisfactory results (Col. 3).

3. Only 29 well cases were found with over 75% of the well length predicted to be in bubble flow. The model performed second best to the Hasan and Kabir mechanistic model for bubble flow (Col. 6).

4. The performance of the slug flow model is exceeded by the Hagedorn and Brown correlation when the Hagedorn and Brown data are included in the data bank (Cols. 7 and 8). The model performed best when Hagedorn and Brown data are not included for all well cases and all vertical well cases (Cols. 9 and 10).

5. The performance of the annular flow models is significantly better than all other methods (Col. 11).

6. Several variables in the mechanistic model, such as bubble rise velocities and film thickness, are dependent on pipe inclination angle. Modifications to include inclination angle effects on these variables should further improve model performance.

References

1. Ozon, P.M., Ferschneider, G., and Chwetzoff, A.: "A New Multiphase Flow Model Predicts Pressure and Temperature Profiles," paper SPE 16535 presented at the 1987 SPE Offshore Europe Conference, Aberdeen, Sept. 8–11, 1987.
2. Hasan, A.R. and Kabir, C.S.: "A Study of Multiphase Flow Behavior in Vertical Wells," *SPEPE* (May 1988) 263.
3. Taitel, Y., Barnea, D., and Dukler, A.E.: "Modelling Flow Pattern Transitions for Steady Upward Gas-Liquid Flow in Vertical Tubes," *AIChE J.* (1980) **26,** 345.
4. Barnea, D., Shoham, O., and Taitel, Y.: "Flow Pattern Transition for Vertical Downward Two-Phase Flow," *Chem. Eng. Sci.* (1982) **37,** 741.
5. Barnea, D.: "A Unified Model for Predicting Flow-Pattern Transition for the Whole Range of Pipe Inclinations," *Intl. J. Multiphase Flow* (1987) **13,** 1.
6. Harmathy, T.Z.: "Velocity of Large Drops and Bubbles in Media of Infinite or Restricted Extent," *AIChE J.* (1960) **6,** 281.
7. Scott, S.L. and Kouba, G.E.: "Advances in Slug Flow Characterization for Horizontal and Slightly Inclined Pipelines," paper SPE 20628 presented at the 1990 SPE Annual Technical Conference and Exhibition, New Orleans, Sept. 23–26.
8. Caetano, E.F.: "Upward Vertical Two-Phase Flow Through an Annulus," PhD dissertation, U. of Tulsa, Tulsa, OK (1985).
9. Zuber, N. and Hench, J.: "Steady State and Transient Void Fraction of Bubbling Systems and Their Operating Limits. Part 1: Steady State Operation," General Electric Report 62GL100 (1962).
10. Fernandes, R.C., Semait, T., and Dukler, A.E.: "Hydrodynamic Model for Gas-Liquid Slug Flow in Vertical Tubes," *AIChE J.* (1986) **29,** 981.
11. Sylvester, N.D.: "A Mechanistic Model for Two-Phase Vertical Slug Flow in Pipes," *ASME J. Energy Resources Tech.* (1987) **109,** 206.
12. McQuillan, K.W. and Whalley, P.B.: "Flow Patterns in Vertical Two-Phase Flow," *Intl. J. Multiphase Flow* (1985) **11,** 161.
13. Brotz, W.: "Uber die Vorausberechnung der Absorptionsgesch-windigkeit von Gasen in Stromenden Flussigkeitsschichten," *Chem. Ing. Tech.* (1954) **26,** 470.
14. Schmidt, Z.: *Experimental Study of Gas-Liquid Flow in a Pipeline-Riser System,* MS thesis, U. of Tulsa, Tulsa (1976).
15. Vo, D.T. and Shoham, O.: "A Note on the Existence of a Solution for Two-Phase Slug Flow in Vertical Pipes," *ASME J. Energy Resources Tech.* (1989) **111,** 64.
16. Dukler, A.E., Maron, D.M., and Brauner, N.: "A Physical Model for Predicting the Minimum Stable Slug Length," *Chem. Eng. Sci.* (1985) 1379.
17. Wallis, G.B.: *One-Dimensional Two-Phase Flow,* McGraw-Hill Book Co. Inc., New York City (1969).
18. Hewitt, G.F. and Hall-Taylor, N.S.: *Annular Two-Phase Flow,* Pergamon Press, Houston (1970).
19. Whalley, P.B. and Hewitt, G.F.: "The Correlation of Liquid Entrainment Fraction and Entrainment Rate in Annular Two-Phase Flow," UKAEA Report AERE-R9187, Harwell (1978).
20. Alves, I.N. *et al.*: "Modeling Annular Flow Behavior for Gas Wells," paper presented at the 1988 Winter Annual Meeting of ASME, Chicago, Nov. 27–Dec. 2.
21. Lopes, J.C.B. and Dukler, A.E.: "Droplet Entrainment in Vertical Annular Flow and Its Contribution to Momentum Transfer," *AIChE J.* (1986) 1500.
22. Govier, G.W. and Fogarasi, M.: "Pressure Drop in Wells Producing Gas and Condensate," *J. Cdn. Pet. Tech.* (Oct.–Dec. 1975) 28.
23. Asheim, H.: "MONA, An Accurate Two-Phase Well Flow Model Based on Phase Slippage," *SPEPE* (May 1986) 221.
24. Chierici, G.L., Ciucci, G.M., and Sclocchi, G.: "Two-Phase Vertical Flow in Oil Wells—Prediction of Pressure Drop," *JPT* (Aug. 1974) 927.
25. Poettmann, F.H. and Carpenter, P.G.: "The Multiphase Flow of Gas, Oil and Water Through Vertical Flow Strings with Application to the Design and Gas-Lift Installations," *Drill. & Prod. Prac.,* API, Dallas (1952) 257.

26. Fancher, G.H., and Brown, K.E.: "Prediction of Pressure Gradients for Multiphase Flow in Tubing," *Trans.*, AIME (1963) **228**, 59.

27. Hagedorn, A.R.: "Experimental Study of Pressure Gradients Occurring during Continuous Two-Phase Flow in Small Diameter Vertical Conduits," PhD dissertation, U. of Texas, Austin (1964).

28. Baxendell, P.B.: "The Calculation of Pressure Gradients in High Rate Flowing Wells," *JPT* (Oct. 1961) 1023.

29. Orkiszewski, J.: "Predicting Two-Phase Pressure Drops in Vertical Pipes," *JPT* (June 1967) 829.

30. Espanol, H.J.H.: "Comparison of Three Methods for Calculating a Pressure Traverse in Vertical Multi-Phase Flow," MS thesis, U. of Tulsa, Tulsa, OK (1968).

31. Messulam, S.A.G.: "Comparison of Correlations for Predicting Multiphase Flowing Pressure Losses in Vertical Pipes," MS thesis, U. of Tulsa, Tulsa, OK (1970)

32. Camacho, C.A.: "Comparison of Correlations for Predicting Pressure Losses in High Gas-Liquid Ratio Vertical Wells," MS thesis, U. of Tulsa, Tulsa, OK (1970).

33. Duns, H. Jr. and Ros, N.C.J.: "Vertical Flow of Gas and Liquid Mixtures in Wells," *Proc.*, 6th World Pet. Cong. (1963) 451.

34. Brill, J.P.: "Discontinuities in the Orkiszewski Correlation for predicting pressure Gradients in Wells," *J. Energy Res. Tech.* (March, 1989) **41**, 34.

35. Beggs, H.D. and Brill, J.P.: "A Study of Two-Phase Flow in Inclined Pipes," *JPT* (May 1973) 607.

36. Palmer, C.M.: "Evaluation of Inclined Pipe Two-Phase Liquid Holdup Correlations Using Experimental Data," MS thesis, U. of Tulsa, Tulsa, OK (1975).

37. Mukherjee, H. and Brill, J.P.: "Pressure Drop Correlations for Inclined Two-Phase Flow," *J. Energy Res. Tech.* (Dec. 1985).

38. Aziz, K., Govier, G.W., and Fogarasi, M.: "Pressure Drop in Wells Producing Oil and Gas," *J. Cdn. Pet. Tech.* (July–Sept. 1972) 38.

39. Kabir, C.S. and Hasan, A.R.: "Performance of a Two-Phase Gas/Liquid Flow Model in Vertical Wells," *JPSE* (1990) **4**, 273.

40. Ansari, A.M. *et al.*: "Supplement to paper SPE 20630, A Comprehensive Mechanistic Model for Upward Two-Phase Flow in Wellbores," paper SPE 28671 available at SPE headquarters, Richardson, TX.

Nomenclature

a = coefficient defined in Eq. 55
A = cross-sectional area of pipe, L, m^2
b = coefficient defined in Eq. 56
c = coefficient defined in Eq. 57
C = constant factor relating friction factor to Reynolds number for smooth pipes
C' = coefficient defined in Eq. 48
d = pipe diameter, L, m
e = error function
E_1 = average percentage error, %
E_2 = absolute average percentage error, %
E_3 = standard deviation, %
E_4 = average error, m/Lt^2, psi
E_5 = absolute average error, m/Lt^2, psi
E_6 = standard deviation, m/Lt^2, psi
f = friction factor
F_E = fraction of liquid entrained in gas core
F_{rp} = relative performance factor, defined in Eq. 112
g = gravity acceleration, m/s^2
h = local holdup fraction
H = average holdup fraction
L = length along the pipe, m
n = number of well cases
n' = exponent to account for the swarm effect on bubble rise velocity

N_{Re} = Reynolds number
p = pressure, m/Lt^2, psi
q = flow rate, L^3/t m^3/s
S = wetted perimeter, L, m
v = velocity, L/t m/s
V = volume, L^3, m^3
X = Lockhart and Martinelli parameter
Y = Lockhart and Martinelli parameter
Z = empirical factor defining interfacial friction
β = length ratio, defined in Eq. 31
δ = film thickness, L, m
δ = ratio of film thickness to diameter
$\bar{\Delta}$ = difference
ε = absolute pipe roughness, L, m
θ = angle from horizontal, rad or deg
λ = no-slip holdup fraction
μ = dynamic viscosity, kg/m·s, kg/m^{-s}
ν = kinematic viscosity, L^2/t, m^2/sq
ρ = density, m/L^3, kg/m^3
σ = surface tension, m/t^2, dyne/cm
τ = shear stress, m/Lt^2, N/m^3
ϕ = dimensionless groups defined in Eqs. 94 and 95

Subscripts

a = acceleration
A = average
c = Taylor bubble cap, core
$crit$ = critical
e = elevation
f = friction
F = film
g = gas
H = hydraulic
i = ith element
I = interfacial
L = liquid
LS = liquid slug
m = mixture
M = modified
max = maximum
min = minimum
N = Nusselt
p = pipe
r = relative
s = slip
S = superficial
SU = slug unit
t = total
TB = Taylor bubble
TP = two-phase

Superscript

* = developing slug flow

SI Metric Conversion Factor

in. $\times 2.54$*   E+00 = cm

*Conversion factor is exact.   **SPEPF**

A.M. Ansari, a senior petroleum engineer, joined Pakistan Petroleum Ltd. in 1989. He holds a BS degree in mechanical engineering from NED U., Karachi, and an MS degree in petroleum engineering from the U. of Tulsa. Nicholas D. Sylvester is dean of engineering at the U. of Akron. He holds a BS degree from Ohio U. and a PhD degree from Carnegie-Mellon U., both in chemical engineering. Previously he served as dean of engineering and applied sciences and chairman of petroleum engineering at the U. of Tulsa. Sylvester has numerous publications in the areas of two-phase and non-Newtonian fluid flow as well as oil field pollution control. Cem Sarica is a research associate in the petroleum engineering department at the U. of Tulsa. He holds BS and MS degrees in petroleum engineering from Istanbul Technical U., and a PhD degree in petroleum engineering from the U. of Tulsa. He was an assistant professor of petroleum engineering at Istanbul Technical U. before joining the U. of Tulsa. His research interests are multiphase flow in pipes, oil and gas production, and fluid flow in porous media. Ovadia Shoham is an associate professor of petroleum engineering at the U. of Tulsa. He received his PhD degree in mechanical engineering from Tel Aviv U., his MS degree in chemical engineering from the U. of Houston, and his BS degree in chemical engineering from the Technion in Israel. Shoham currently teaches and conducts research in the area of modeling two-phase flow in pipes and its application in oil and gas production, transportation, and separation. He has over fifty publications in the areas of two-phase flow and production operations. Shoham served in several capacities in the Tulsa U. Fluid Flow Projects (1982–1991), including Director of Research. He was a member of the Production Operation Technical Committee (1990–1992) and served as a member of the planning committee of the Forum Series on Multiphase Flow in 1992. James P. Brill is the F.M. Stevenson professor of petroleum engineering at the U. of Tulsa and founder and Executive Director of the Tulsa U. Fluid Flow Projects. He holds a BS degree from the U. of Minnesota and a PhD in petroleum engineering from the U. of Texas at Austin. He currently teaches and conducts research in the areas of two-phase flow in pipes and production design and has published extensively in these areas. Brill was a member of the Distinguished Lecturer Committee, a 1982 Distinguished Lecturer, 1978–81 Engineering Manpower Committee member, a member of the Education and Professionalism Committee for the 1971 and 1976 Annual Meetings, and a member of the Education and Accreditation Committee during 1967–70. He has served as an SPE representative to the ABET Engineering Accreditation Commission and ex-officio member of the Education and Accreditation Committee since 1990.

Ansari   Sylvester   Shoham

Brill   Sarica